Applied Catalysis B: Environmental 176–177 (2015) 36–43

Contents lists available at ScienceDirect

Applied Catalysis B: Environmental

journal homepage: www.elsevier.com/locate/apcatb

Iodine-modified nanocrystalline titania for photo-catalytic antibacterial application under visible light illumination

Huaxiang Lin, Weihua Deng, Tanghua Zhou, Shangbo Ning, Jinlin Long*, Xuxu Wang*

State Key Laboratory of Photocatalysis on Energy and Environment, School of Chemistry, Fuzhou University, Fuzhou 350002, PR China

ARTICLE INFO

Article history:
Received 20 January 2015
Received in revised form 17 March 2015
Accepted 23 March 2015
Available online 24 March 2015

Keywords:
Iodine-modified TiO_2
Antibacterial
Photocatalysis
Visible light illumination

ABSTRACT

Iodine-modified TiO_2 nanocrystallites (denoted as I-TiO_2) were synthesized by a combination of sol-gel process (TiO_2 sol) and solvothermal method in the presence of HI solution. Their photocatalytic and anti-bactericidal activities were systematically investigated under visible light irradiation. The results showed that the iodine modifier existed in the form of I_2 is responsible for the visible light response. Moreover, the I_2 significantly enhanced the antibacterial activity under visible light and was stable during the photocatalytic process. In addition, an interesting post-illumination catalytic memory of I-TiO_2 that continues to inhibit the growth of *Escherichia coli* in dark was also observed after the visible light was shut off.

1. Introduction

Despite TiO_2 has been extensively used in environmental and clean energy fields due to its highly active, low toxicity, chemical stability, biocompatibility and inexpensiveness [1–10], using TiO_2 particles as antibacterial agent in biomedical applications has received considerable attention because of its long-acting antibacterial properties under UV light illumination [11–13]. The antibacterial effect of TiO_2 was first applied in biomedical application by Cai in the immortal HeLa cell lines [1].

However, TiO_2 and some TiO_2-based photocatalyst can only be excited by UV light [6,14–16], which greatly limits its biomedical application under visible-light or normal room light illumination. Search for high efficient antibacterial photocatalyst under visible light (VL) has been an intensively pursued topic in the field of photocatalysis research. Generally, two major approaches have been frequently employed to fabricate visible-light-driven (VLD) photocatalyst. One is to purposely fabricate new forms of VLD photocatalyst, such as Cu_2O/SiC [17], $LaVO_4$/g-C_3N_4 [18], $(Ag_{0.75}Sr_{0.25})(Nb_{0.75}Ti_{0.25})O_3$ [19], $C_3N_3S_3$ [20], and N-Modified $BiWO_6$ [21], etc. Another is to modify TiO_2 with elements such as C, N, S, F, B, Fe, Bi and I [2,15,22–34], to extend the light absorption spectrum of TiO_2 from the UV to VL region. Among these nonmetal impurities, iodine-modified TiO_2 nanocrystallites have been received more attention because iodine-doping not only alters the surface charge and bulk band gap of TiO_2, which causes the photo-response of TiO_2 to enlarge from UV to VL region, but also sufficiently reduces the recombination of photogenerated electron–hole(e^-–h^+) by trapping the photogenerated electrons [35–44]. I-modified TiO_2 has been reported enhance visible-light photocatalytic activities in the degradation of organic pollutant such as methyl orange [45], 4-CP [13], phenol [46], acetone [39] and RhB [47]. However, there are little reports about the antibacterial activity of iodine-modified TiO_2 nanocrystallites under visible light and the stability of iodine-modified TiO_2 during the photocatalytic process has not been well demonstrated. In addition, no experimental evidence has been given on the post-illumination catalytic memory of iodine-modified TiO_2 in dark, a characteristic that has great importance in the practical applications [48–50].

In this work, iodine-modified TiO_2 nanocrystallites samples with different amount iodine were prepared by a combination of sol–gel process (TiO_2 sol) and solvothermal method. The antibacterial activity and stability of iodine-modified TiO_2 were valued by antibacterial of *Escherichia coli* and photocatalytic degradation of RhB under VL for multiple cycle tests. The chemical states of iodine-modified TiO_2 before and after photocatalytic reaction were characterized by XPS. By further detecting the generation of •O2− and OH species, the plausible mechanism of photocatalytic antibacterial activity and the post-illumination catalytic memory of iodine-modified TiO_2 in dark are discussed. It is hoped that our work helps better understanding of the role of the iodine-modifier in the photocatalytic antibacterial activity of TiO_2, and also provides

* Corresponding authors. Tel.: +86 591 83779121.
E-mail addresses: jllong@fzu.edu.cn (J. Long), xwang@fzu.edu.cn (X. Wang).

http://dx.doi.org/10.1016/j.apcatb.2015.03.039
0926-3373/

a method to obtain highly visible photoactive and antibacterial photocatalysts.

2. Experimental

2.1. Catalyst preparation

2.1.1. Materials and Reagents

RhB ($C_{28}H_{31}C_lN_2O_3$) was purchased from Beijing Chemical Reagents Company. The bacterial cells were cultured in nutrient broth (BioLife, Milano, Italy) solution at 37 °C for 18 h and immediately diluted. The concentration of cell density is 10^7 cfu (colony forming unit)/ml. TiO_2 sol (Research Institute of Photocatalysis, State Key Laboratory Breeding Base, Fuzhou University, Fuzhou, China) was used as the Ti source. Hydroiodic acid (HI, ≧45%, Sinopharm Chemical Reagent Co., Ltd., Shanghai) was used as the iodine source. Furfural (The morning chemical reagent factory in Tianjin) was used as template. All these reagents were of analytical grade and used as received. Millipore water with a resistivity of 18.2 MΩ was used throughout the study. All of used glass apparatuses were washed with millipore water, and then autoclaved at 121 °C for 15 min.

2.1.2. Synthesis of TiO_2

50 mL of titanium oxide sol and 25 mL of furfural (65–68%) were mixed and stirred at room temperature for 4 h. Then the color of TiO_2 sol changes from blue to brown. The brown solution was transferred to a Teflon-lined autoclave and reacted at 160 °C for 12 h, after that time a black resin was formed. Finally, the black resin was heated at 450 °C in air for 36 h to remove furfural and a white cotton-like product was obtained. In this work, the furfural acts as template agent to inhibit agglomeration of TiO_2 at 450 °C and enlarge the surface area of TiO_2.To compare, TiO_2 powder was prepared by the same method as above only without adding furfural.

2.1.3. Synthesis of iodine-modified TiO_2 (I-TiO_2)

Iodine-modified TiO_2 was prepared as follows: first, different amounts of hydroiodic acid were dissolved in 25 mL absolute ethanol. The TiO_2-iodine suspension was obtained by mixing TiO_2 and the above hydroiodic acid solution with the molar ratios of HI to TiO_2 of 0.4, 0.8, 1.6, respectively. After stirring at room temperature for 4 h, the three suspensions were transferred into Teflon-lined autoclave to solvothermal treatment at 160 °C for 12 h. Finally, the obtained suspensions were filtered and the resultant powders were washed with distilled water and then dried at 80 °C for 12 h to get iodine-modified TiO_2 powders. For ease of presentation, the corresponding samples were labeled as 0.4I-TiO_2, 0.8I-TiO_2, and 1.6I-TiO_2, respectively.

2.2. Characterizations

The crystal structure was analyzed by X-ray diffraction (XRD) on a DMAX-2400 (Rigaku, Japan, Cu Kα, λ = 0.15406 nm) radiation at 56 kV and 182 mA with a secondary graphite crystal monochromator. The morphologies were observed by a scanning electron microscopy (SEM, HITACHI S-4700) and high-resolution transmission electron microscopy (HRTEM). HRTEM analysis was performed on a JEOL 2200FS (JP) microscope, with a field emission gun, operated at 300 kV and equipped with energy-dispersive X-ray (EDX) analyzer (Oxford Instruments, Abingdon, U.K.). Samples were prepared by suspending and sonicating the powders in isopropyl alcohol and then placing sonicating evaporating a drop of the suspension on a carbon-coated copper grid. The surface area, pore textures, and size distributions were characterized on a Micromeritics ASAP 2020 system by the N_2 adsorption–desorption experiment. Pore diameter and volumes were calculated from the desorption branch of the Barret–Joyner–Halenda (BJH) model. The optical absorption properties were evaluated on Carry 500 UV/vis/NIR spectrometer that equipped with an integrated sphere attachment using $BaSO_4$ as the reference. The X-ray photoelectron spectroscopy (XPS) measurements of the samples were carried out on a ESCALAB 250 photoelectron spectrometer (Thermo Fisher Scientific) at 3.0×10^{-10} mbar with monochromatic Al Kα radiation (E = 1486.2 eV). To detect the generation of activated species, spin-trapping electron spin resonance (ESR) measurements were conducted on a Bruker model A300 spectrometer. Transient photocurrent characterization was conducted on a ZENNIUM electrochemical workstation (Zahner, Germany) with a standard three-electrode system under visible light irradiation. The prepared samples served as the working electrode with an active area of ca. 0.25 cm^2. The counter and reference electrodes were Pt plate and Ag/AgCl electrode and 0.2 M Na_2SO_4 (pH 6.8) was used as electrolyte.

2.3. Visible-light-driven photodegradation/antibacterial activity

The photocatalytic activity of the prepared samples was evaluated by measuring the photocatalytic degradation of RhB and phenol. In order to evaluate the VL induced photocatalytic activity, 50 mg powers were put into a pyrex glass reactor and 80 mL RhB (10 ppm) was added. A 300 W Xe lamp was used with cut-off filter to provide visible light (≥420 nm). Prior to irradiation, the suspensions were magnetically stirred in the dark for 30 min to establish the adsorption–desorption equilibrium. At given irradiation time intervals, 4 mL of the solution were taken out and centrifuged, then analyzed on the UV–vis spectrometer (Cary 500). The final efficiency was calculated by the following equation:

$$E_t(\%) = (1 - C_t/C_0) \times 100\%,$$

where C_0 and C_t stand for the concentration of reactants at initial and at a certain irradiation time, respectively.

The antibacterial activity was estimated by killing of *E. coli* under visible light irradiation. 5 mL of *E. coli* suspension (1.0×10^7 cfu/mL) and 45 mL of a phosphate buffer solution were pipetted into a container and 50 mg catalyst powers were added. At given irradiation time intervals, 0.5 mL of the solution were taken out and centrifuged, and spread on freshly prepared agar plates, and incubated at 37 °C for 48 h, then, the number of viable cells in terms of colony-forming units was counted.

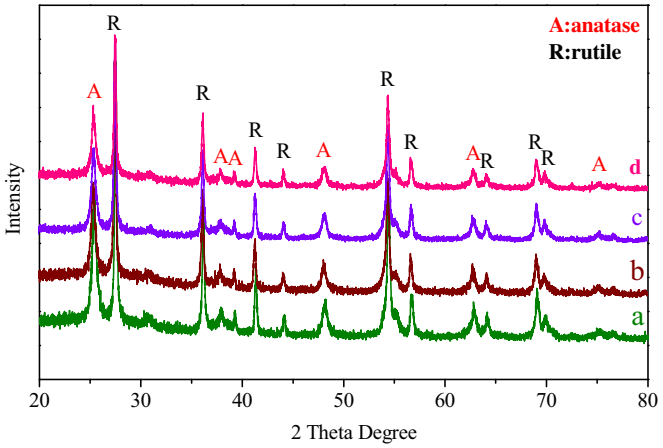

Fig. 1. XRD patterns of (a) TiO_2, (b) 0.4I-TiO_2, (c) 0.8I-TiO_2, (d) 1.6I-TiO_2.

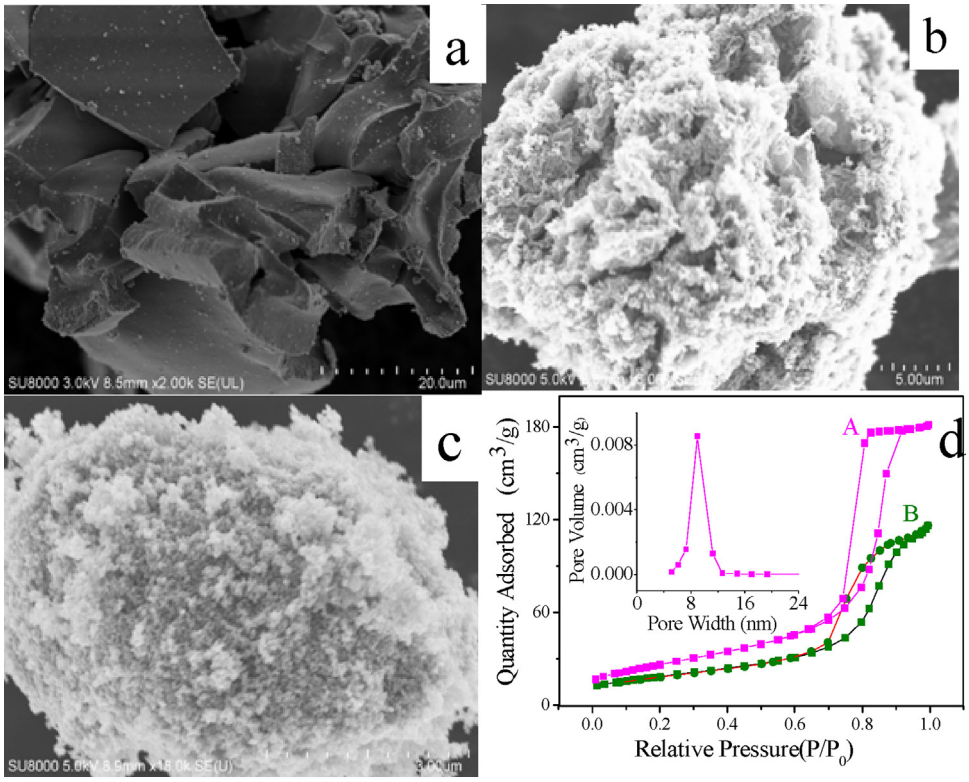

Fig. 2. SEM images of (a) TiO_2 (without furfural), (b) TiO_2 (with furfural), (c) 0.8I-TiO_2, (d) BET of 0.8I-TiO_2 (A: with furfural, B: without furfural).

3. Results and discussion

3.1. Characterization of as-synthesized samples

Fig. 1 shows the XRD spectra of the un-modified TiO_2 that was baked at 450 °C (line a) and as-synthesized I-TiO_2 samples with different amount of I (line b, c, d), respectively. For both TiO_2 and I-TiO_2, a series of characteristic peaks at 25.2° (1 0 1), 37.9° (0 0 4), 47.9° (2 0 0), and 62.6° (2 0 4) are observed that are indexed to anatase TiO_2 (JCPDS file No. 21-1272), and the peaks at 27.4° (1 1 0), 36.1°(1 0 1), 41.2° (1 1 1), and 44.04° (2 1 0), 54.3° (2 1 1), 56.65° (2 2 0) belong to rutile TiO_2 (JCPDS file No. 21-1276) [38]. However, no peaks of iodine could be observed for I-TiO_2 sample, probably due to the low content of iodine in this composite photocatalyst which is below the detection limit of XRD technique.

Fig. 2 shows the SEM image of the pure TiO_2 prepared under different conditions and iodine-modified TiO_2. Compared to the TiO_2 that without adding furfural (Fig. 2a), the morphologies of TiO_2 treated with furfural were found to be like "sponge". Also, iodine deposition brought no observable change to the morphology of TiO_2 samples (Fig. 2c). In addition, after treated with furfural, the BET surface area of the samples is enhanced from 64.8 to 97.19 m^2/g (Fig. 2d), which indicates that the furfural plays crucial roles in the formation of the sponge's networks and enlargement of surface area. The TEM image of 0.8I-TiO_2 (Fig. 3a) shows that the diameter of 0.8I-TiO_2 particles was about 30–100 nm. The EDX characterization (Fig. 3b) confirms that the as-synthesized samples are composed of only titanium, oxygen and iodine. The Ti, O, and I contents in the sample are calculated about 37.1, 62.5, and 0.367 at.%, respectively.

To study the chemical states of iodine on I-TiO_2, XPS analysis of TiO_2 and I-TiO_2 was carried out. Fig. 4a shows XPS survey spectrum of 0.8I-TiO_2, indicating the existence of Ti, O, and I elements. The high resolution XPS spectra of Ti 2p region around 460 eV (Fig. 4b), I 3d region around 620 eV (Fig. 4c), and the O 1s region around 530 eV (Fig. 4d) were analyzed, respectively. As seen in Fig. 4b,

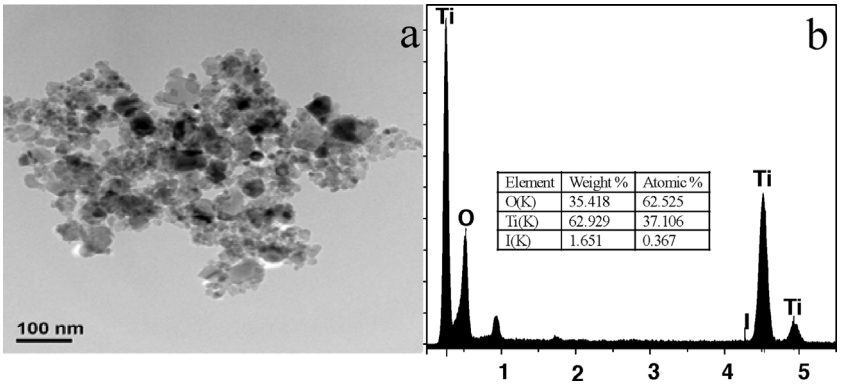

Fig. 3. (a) TEM images of the 0.8I-TiO_2, (b) the corresponding EDX spectrum images of 0.8I-TiO_2.

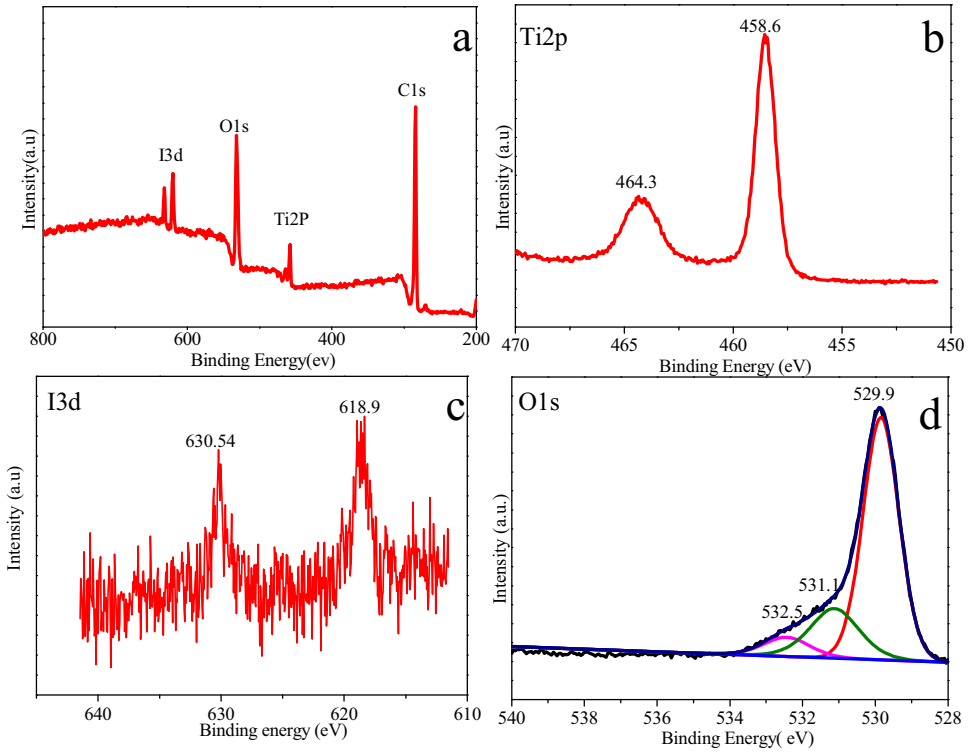

Fig. 4. XPS analysis of the 0.8I-TiO2 composite photocatalyst: (a) overall XPS spectra; (b) Ti 2p; (c) I 3d and (d) O 1s.

the two peaks located at 458.5 and 464.2 eV can be assigned to the core levels of Ti^{4+} 2p3/2 and Ti^{4+} 2p1/2, respectively. The XPS spectrum of the I 3d region in Fig. 4c shows two peaks at 618.9 eV and 630.6 eV that can be ascribed to I 3d 5/2 and I 3d 3/2 binding energies, respectively. These observations confirm the existence of zero-valent iodine on the surface of 0.8I-TiO_2, suggesting that the iodine modifier exists in the form of I_2 or $(I_2)_n$ [51,52]. Additionally, after curve fitting, the high resolution XPS peaks of the O 1s region show a strong peak at 529.9 eV that was attributed to lattice oxygen of TiO_2 (Fig. 4d) [41,52–54]. Besides the main peak of O 1s located at 529.9 eV, the shoulder peaks located at 531.3 and 532.5 eV could be ascribed to the surface species such as hydroxyl groups (O_{OH}) or Ti—OH and Ti—O—O—, respectively [53,55,56].

Fig. 5 shows the UV–vis diffuse reflectance spectra (UV–vis DRS) of pure TiO_2 and as synthesized I-TiO_2. It is clearly seen that the presence of iodine extended photoabsorption of TiO_2 to visible light region. The I-TiO_2 demonstrated a much enhanced light absorption in the visible region between 400 and 600 nm, compared to the pure TiO_2. On the one hand, this great absorption in visible light may be due to yellow color of the sample induced by iodine (insert in Fig. 5). On the other hand, the sharp increase in absorbance and the absorption tail in visible light region of I-TiO_2 was attributed to band narrowing and surface defect states on TiO_2 caused by iodine modification [46,52,57–59].

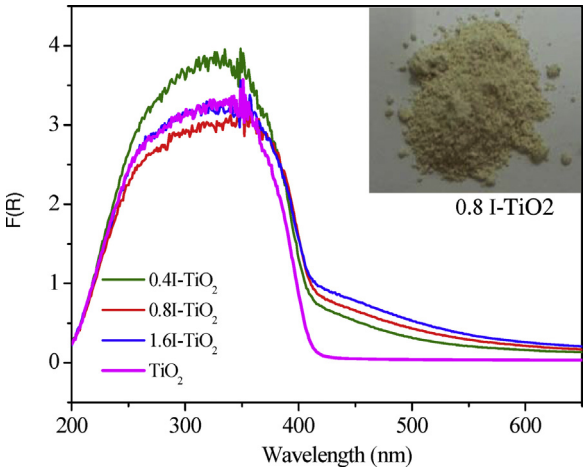

Fig. 5. UV–vis DRS spectra of TiO_2 and A series of I-TiO_2 composite photocatalysts (inset: photo of 0.8I-TiO_2).

3.2. Photocatalytic activity under visible light illumination

To compare the photocatalytic activities and stability of TiO_2 and I-TiO_2, we first examined the photocatalytic degradation of RhB upon visible-light irradiation as shown in Figs. 6 and 7, respectively. There are no obvious changes in the concentration of RhB in the dark and only with visible-light irradiation. Little change in the concentration of RhB during visible-light irradiation process indicates that the pure TiO_2 has little visible-light photocatalytic activity through an indirect dye photosensitization degradation process. However, for I-TiO_2, the concentration of RhB decreases quickly, especially the 0.8I-TiO_2 exhibits the best photocatalytic activity (insert in Fig. 6a line0.8I-TiO_2). The absorption spectra and color change of RhB solution at various-irradiation times are shown in Fig. 6b. The characteristic absorption of RhB at 553 nm almost disappears after 15 min, and the weak absorption at 500 nm, which can be assigned to intermediate product of RhB [60,61], appears. Simultaneously, the color of RhB solution changes from initial pink-red to light yellow. After irradiated under visible light for 60 min, the characteristic absorption of RhB completely disappears and the color changes to colorless, which demonstrates that the deep oxidation occurs concurrently during the photo-degradation.

The photocatalytic stability of the 0.8I-TiO_2 was investigated by six cycling runs and the results are shown in Fig. 7. The 0.8I-TiO_2 catalyst can be effectively recycled at least six times under

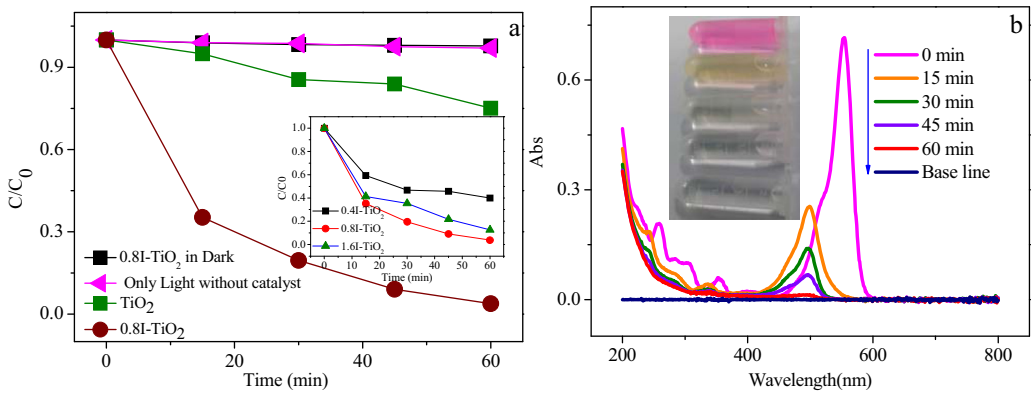

Fig. 6. (a) Photocatalytic degradation of RhB with various catalysts under Visible Light irradiation. (b) Spectral changes of 0.8I-TiO_2 with reaction time.

VL irradiation without an apparent decrease in its photocatalytic activity, which demonstrates its high stability.

3.3. Photocatalytic antibacterial activity under visible light illumination

The sterilization activity of the pure TiO_2 and iodine-modified TiO_2 were valued by their photocatalytic disinfection effect on *E. coli*, which was investigated by exposing the *E. coli* suspended in buffer solution in the presence of photocatalyst under visible light illumination for varying time intervals. Fig. 8 shows the survival ratio of *E. coli* versus VL irradiation time under different conditions. When there was only in light irradiation (without catalyst), the cell density of *E. coli* increased slightly with increasing time. Upon the presence of pure TiO_2, a weak *E. coli* disinfection is observed under visible light illumination. After irradiation for 6 h, the cell density of *E. coli* is about at 3.3×10^5 cfu/mL, which could be due to the weak photocatalytic activity of pure TiO_2 under visible light illumination. Without light illumination, the 0.8I-TiO_2 exhibits no antibacterial activity. The cell density of *E. coli* remains at 4.8×10^7 cfu/ml, which indicates that the 0.8I-TiO_2 have no toxic effect. Under visible light illumination, however, the 0.8I-TiO_2 showed a much better disinfection effect on *E. coli* than pure TiO_2. The cell density of *E. coli* continuously decreased with the increase of irradiation time. After irradiation for 6 h, the cell density of *E. coli* decreased to 8.1×10^2 cfu/mL. The other I-TiO_2 (0.4I-TiO_2 and 1.6I-TiO_2) exhibit slightly different antibacterial activity as can be seen in (insert in Fig. 8).

The stability of a photocatalyst plays an important role on its practical applications. Fig. 9 shows the cell density of *E. coli* by 0.8I-TiO_2 under visible light illumination for six runs. After one run, the sample was collected, washed twice with distilled water and dried at 80 °C, and then reused for photocatalytic antibacterial experiment for the next run. The 0.8I-TiO_2 exhibits similar disinfection effect under visible light illumination for the six runs. The cell density of *E. coli* was about 3.4×10^3 cfu/mL after illumination for 6 h and no obvious reduction of the antibacterial efficiency was observed, which indicated that the 0.8I-TiO_2 was stable in the photocatalytic antibacterial process.

The iodine modified TiO_2 had been reported to be instable during the photocatalytic process and iodine can exist in different oxidation states [39,40,47,62]. In our work, the stability of antibacterial activity of 0.8I-TiO_2 confirms that the iodine modifier was stable. The high resolution XPS scans of I 3d peaks before and after the photocatalytic disinfection of *E.coli* for six runs are shown in Fig. S1. It can be seen that the 3d5/2 and 3d3/2 binding energies have no changes, further indicating the good stability of the 0.8I-TiO_2 photocatalyst.

In addition, an interesting phenomenon was observed for the 0.8I-TiO_2 that demonstrates sustainable antibacterial effect of *E. coli* in the dark. In this work, the 0.8I-TiO_2 catalyst was suspended in buffer solution with *E. coli* and illuminated under visible light for ~6 h. Then, the lamp was shut off and the buffer solution was kept in dark for 48 h. To comparison, the 0.8I-TiO_2 catalyst without pre-illumination was used to conduct antibacterial experiments in the dark. Fig. 10 shows the change of cell density of *E. coli* with and

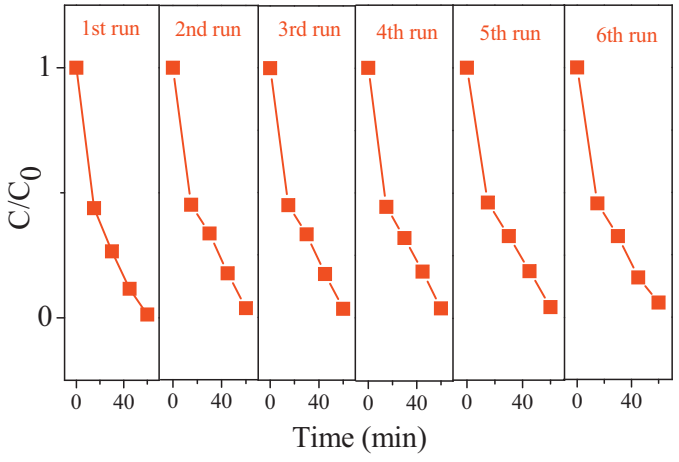

Fig. 7. Six cycling runs in the degradation of RhB catalyzed with 0.8I-TiO_2 under visible light irradiation.

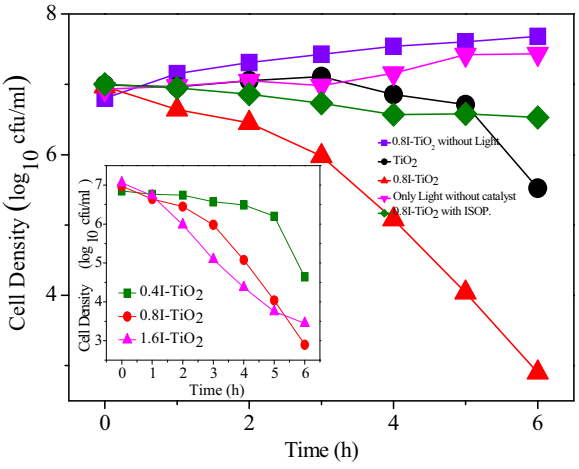

Fig. 8. Photocatalytic inactivation of *E. coli* (1×10^7 cfu/mL) with TiO_2 or 0.8I-TiO_2 (inset: I-TiO_2 of different iodine concentrations) under visible light irradiation.

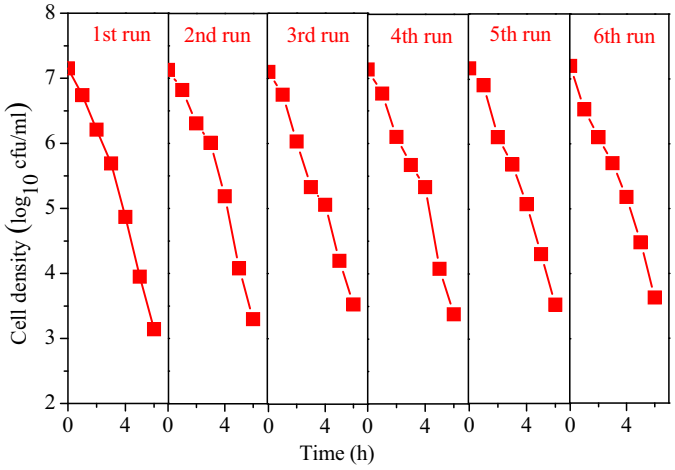

Fig. 9. Six cycling runs in the *E. coli* photocatalytic inactivation with 0.8I-TiO_2 under visible light irradiation.

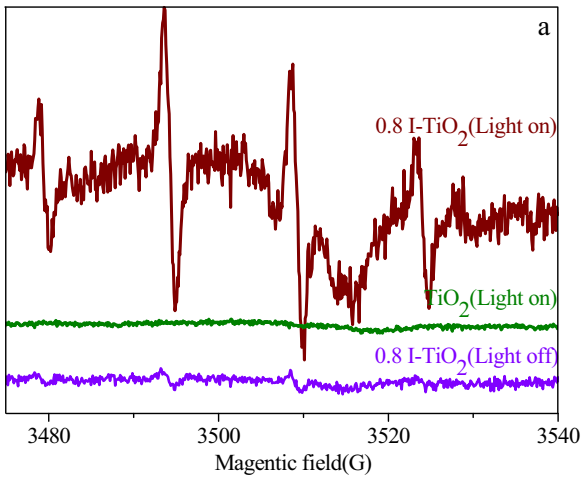

Fig. 11. DMPO spin-trapping ESR spectra recorded at ambient temperature in TiO_2 or 0.8I-TiO_2 suspension under visible light irradiation: For DMPO-•OH in aqueous dispersion.

without pre-illumination for ~6 h and then kept in dark for 48 h. After pre-illumination for 6 h and then kept in dark for 48 h, the cell density of *E. coli* decreased to 1.31×10^2 cfu/mL. However, the cell density of *E. coli* in 0.8I-TiO_2 catalyst that without pre-illumination, increased from 1.6×10^7 cfu/mL to 2.6×10^8 cfu/mL in the dark. This fact indicates that the 0.8I-TiO_2 catalyst could effectively inhibit the growth of *E. coli* in the dark even after the lamp was shut off. The phenomenon that the photocatalyst retains active even after the lamp was shut off was named post-illumination catalytic memory by previous reports [48–50]. This post-illumination catalytic memory was generally observed on some composite catalyst base on TiO_2 and was attributed to the trapping and release of photo-generated electrons from one component to TiO_2 [34]. In this work, the photo-excited electrons on TiO_2 surface may be trapped by I_2 and then released in the dark to produce radicals, which results in catalytic memory of I-TiO_2. This suggestion will be discussed below.

3.4. Plausible mechanism of photocatalytic activity

The antibacterial mechanism of TiO_2 induced by UV-light has been well-documented [10]. According to previous reports, the reactive oxygen species (ROS) (OH or O^{2-}) produced by photogenerated electron-hole play a crucial role in the photocatalytic killing bacteria. In this work, we compared the generation capability of O_2^- and OH radicals of pure TiO_2 and iodine modified TiO_2 under visible light irradiation. The ESR spin-trap technique (with DMPO) was used to obtain some information on the active radicals. As exhibited in Fig. 11, the four characteristic peaks of the DMPO-OH (1:2:2:1 quartet pattern) are observed for the 0.8I-TiO_2 sample, which demonstrated the ability of 0.8I-TiO_2 to generate OH radicals under visible light irradiation. Furthermore, after the light is shut off, there is still weak peaks of the DMPO-OH (Fig. 11, line 0.8I-TiO_2 light off), which confirms that I-TiO_2 releases the trapped electron in dark. However, no OH signal is detected when the pure TiO_2 is under visible light irradiation. Similarly, the six characteristic peaks of DMPO-O_2^- are also observed for the iodine-modified TiO_2 under visible light irradiation (Figure S2) and no O_2^- signal is detected for the pure TiO_2 under visible light irradiation. In the photocatalytic antibacterial experiment, the 0.8I-TiO_2 exhibits higher disinfection activity than pure TiO_2 (Fig. 8 line ▲0.8I-TiO_2 with light and line ●TiO_2 with light), which is in accordance with the generation capability of O_2^- and OH radicals of iodine-modified TiO_2 and pure TiO_2, respectively. Furthermore, after adding small amount scavenger agent of OH (isopropanol) [63] during the photocatalytic antibacterial experiment, the antibacterial activity of 0.8I-TiO_2 decreases greatly (Fig. 8 line ♦0.8I-TiO_2+isop.). These facts demonstrate that the reactive oxygen species (OH or O_2^-) have much to do with the photocatalytic antibacterial activity of photocatalyst. In addition, the ESR results also indicate that the iodine modifier plays an important role in the production of OH and O_2^- under visible light irradiation.

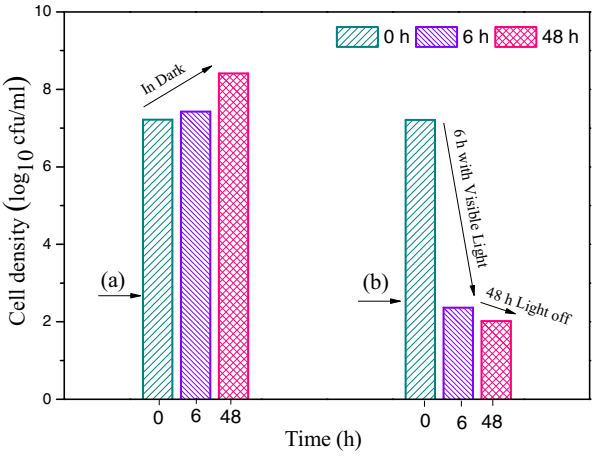

Fig. 10. Survival concentration of *E. coli* bacteria with 0.8I-TNCs photocatalysts: (a) in the dark all the time, (b) After being illuminated under visible light for 6 h, then were put into a dark environment 48 h.

Generally, pure TiO_2 cannot be excited to generate O_2^- and OH radicals under visible light irradiation. Our ESR results further confirm it. After modification with iodine, a continuous state residing between the VB and CB of TiO_2 was induced [42]. As show in Fig. 12, the I-induced continuous state acts as a bridge to transfer visible light excited electrons on the VB of TiO_2 to the CB of TiO_2 and promotes the separation of photo-generated electron-holes pairs of TiO_2. Under visible light irradiation, electrons are excited from the valence band of TiO_2 to I-induced continuous states and holes leave on the valence band of TiO_2. The electrons in the continuous states can be further photo-excited to the conduction band of the semiconductor (TiO_2) and captured by O_2 to produced O_2^-. And the holes staying on the valence band of TiO_2 can oxidize hydroxyl to generate hydroxyl radicals (OH), which can kill bacteria. In addition, the I_2 doped on TiO_2 surface can be also excited to form the excited state by absorbing a visible photon, from which an electron

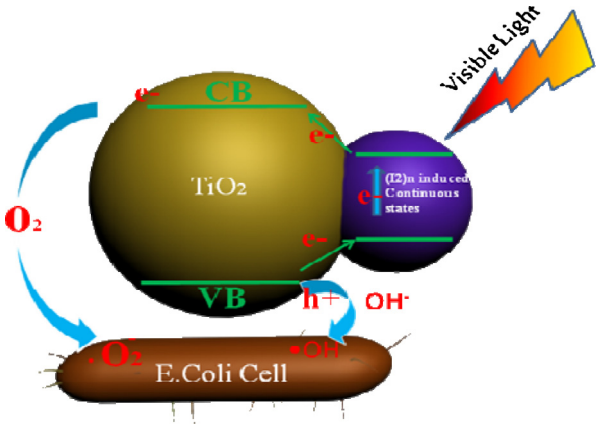

Fig. 12. Schematic drawing of the photocatalytic antibacterial process of I-TiO_2.

can be transferred to the CB of TiO_2 to produce O_2^- as Eqs. (1) and (2).

$$(I_2)_n + h\upsilon \rightarrow (I_2)_n^* \quad (1)$$

$$(I_2)_n^*(e^-) + TiO_2 \rightarrow (I_2)_n + TiO_{2(CB)}(e^-) \quad (2)$$

To confirm the role of I_2 in the promoting the separation of electron-holes pairs of TiO_2, the transient photocurrent response of pure TiO_2 and 0.8I-TiO_2 under visible light and UV light were carried out, which has been demonstrated to be a useful technique for investigating the efficiency of the separation of photogenerated electron-hole pairs [64,65]. Fig. 13 shows a comparison of the *I–t* curves over several on-off cycles of intermittent light irradiation for pure TiO_2 and 0.8I-TiO_2 composites. In common sense, the initial current results from the separation of electron–hole pairs at the TiO_2/electrolyte interface, during which photo-generated holes migrating to TiO_2 surface are trapped or captured by reduced species in the electrolyte while the electrons are transported to the back contact substrate via TiO_2 [51,66]. When under VL irradiation, no obvious photocurrent value was observed on TiO_2 but significant enhancement of the photocurrent occurred on 0.8I-TiO_2. The photocurrent value of 0.8I-TiO_2 was about 9 times higher than that of pure TiO_2 as illustrated in Fig. 13. Similarly, when under UV irradiation, the photocurrent value of 0.8I-TiO_2 was greatly higher than that of TiO_2 as shown in Fig. S3a and Fig. S3b. These results indicate that the modified I_2 greatly promote the charge separation of TiO_2 in the photo-electrochemical process. Also, the current is steady within the whole illumination period, implying that there is little recombination process.

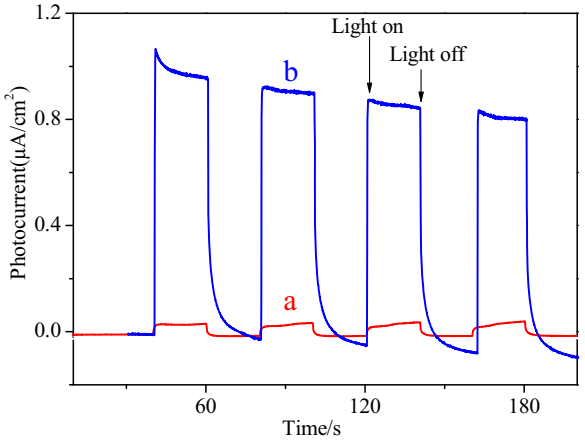

Fig. 13. Transient photocurrent responses of (a) TiO_2 and (b) 0.8I-TiO_2 under visible light irradiation.

The transient photocurrent response of 0.8I-TiO_2 also explains the catalytic memory of I-TiO_2. As can be seen in Fig. 13, when the light is turned off, a gradual decrease of the photocurrent to zero was observed. This phenomenon was ascribed to the electron storage capacity of photocatalyst [65,67]. The trapping and release photogenerated electron enable many photocatalyst to be active even after the light was shut off [49]. In our 0.8I-TiO_2 sterilization activity, the observed antibacterial activity in the dark after the light is turned off (Fig. 10), which may also be attributed to the trapping and release photogenerated electron by 0.8I-TiO_2. After light is turned off, electrons stored on 0.8I-TiO_2 gradually release from 0.8I-TiO_2 and transfer to buffer solution, then generate $O_2\bullet^-$. The $O_2\bullet^-$subsequently reacts with H_2O and produce OH which results in the disinfection of bacteria.

4. Conclusions

In summary, iodine-modified TiO_2 nanocrystallites samples with high visible photokilling activity were prepared by a combination of sol-gel process (TiO_2 sol) and solvothermal method. The iodine modifier presented in the form of I_2 and was stable during the photocatalytic process. The I_2 promoted the visible absorption of TiO_2 and significantly enhanced the visible antibacterial activity. In addition, the I_2 endowed TiO_2 with catalytic memory that remains antibacterial active even after the light was cut off. It was revealed that iodine-modification efficiently enlarge the charge carrier separation of TiO_2.

Acknowledgements

This work was financially supported by NSFC (Grants Nos. 21373051, U1305242, and 21173044), the great Science and Technology Project of Fujian Province of PR China (2012Y4003).

Appendix A. Supplementary data

Supplementary data associated with this article can be found, in the online version, at http://dx.doi.org/10.1016/j.apcatb.2015.03.039.

References

[1] R. Cai, K. Hashimoto, K. Itoh, Y. Kubota, A. Fujishima, Bull. Chem. Soc. Jpn. 64 (1991) 1268–1273.
[2] X. Chen, C. Burda, J. Am. Chem. Soc. 130 (2008) 5018–5019.
[3] D.D. Ramos, P.C. Bezerra, F.H. Quina, R.F. Dantas, G.A. Casagrande, S.C. Oliveira, M.R. Oliveira, L.C. Oliveira, V.S. Ferreira, S.L. Oliveira, Environ. Sci. Pollut. Res. (2014) 1–10.
[4] A.S. Giri, A.K. Golder, Ind. Eng. Chem. Res. 53 (2014) 1351–1358.
[5] M. Anpo, M. Takeuchi, J. Catal. 216 (2003) 505–516.
[6] M. Anpo, H. Yamashita, Y. Ichihashi, S. Ehara, J. Electroanal. Chem. 396 (1995) 21–26.
[7] M. Anpo, H. Yamashita, Y. Ichihashi, Y. Fujii, M. Honda, J. Phys. Chem. B 101 (1997) 2632–2636.
[8] Q. Gu, J. Long, L. Fan, L. Chen, L. Zhao, H. Lin, X. Wang, J. Catal. 303 (2013) 141–155.
[9] K. Mori, H. Yamashita, M. Anpo, RSC Adv. 2 (2012) 3165–3172.
[10] T. Rajh, N.M. Dimitrijevic, M. Bissonnette, T. Koritarov, V. Konda, Chem. Rev. 114 (2014) 10177–10216.
[11] V. Etacheri, G. Michlits, M.K. Seery, S.J. Hinder, S.C. Pillai, ACS Appl. Mater. Interfaces 5 (2013) 1663–1672.
[12] J. Ding, Key Eng. Mater. 575 (2014) 302–305.
[13] A. Kubacka, M.S. Diez, D. Rojo, R. Bargiela, S. Ciordia, I. Zapico, J.P. Albar, C. Barbas, V.A.P. Martins dos Santos, M. Fernandez-Garcia, M. Ferrer, Sci. Rep. 4 (2014) 4134.
[14] K. Sunada, T. Watanabe, K. Hashimoto, Environ. Sci. Tech. 37 (2003) 4785–4789.
[15] J. Schneider, M. Matsuoka, M. Takeuchi, J. Zhang, Y. Horiuchi, M. Anpo, D.W. Bahnemann, Chem. Rev. 114 (2014) 9919–9986.

[16] H. Lin, Z. Xu, X. Wang, J. Long, W. Su, X. Fu, Q. Lin, J. Biomed. Mater. Res. Part B: Appl. Biomater. 87 (2008) 425–431.
[17] H. Li, Y. Lei, Y. Huang, Y. Fang, Y. Xu, L. Zhu, X. Li, J. Nat. Gas Chem. 20 (2011) 145–150.
[18] Y. He, J. Cai, L. Zhang, X. Wang, H. Lin, B. Teng, L. Zhao, W. Weng, H. Wan, M. Fan, Ind. Eng. Chem. Res. 53 (2014) 5905–5915.
[19] D. Wang, T. Kako, J. Ye, J. Am. Chem. Soc. 130 (2008) 2724–2725.
[20] J. Xu, L. Luo, G. Xiao, Z. Zhang, H. Lin, X. Wang, J. Long, ACS Catal. 4 (2014) 3302–3306.
[21] B. Tang, G. Jiang, Z. Wei, X. Li, X. Wang, T. Jiang, W. Chen, J. Wan, Acta Metall. Sin. (Engl. Lett.) 27 (2014) 124–130.
[22] Y. Cong, J. Zhang, F. Chen, M. Anpo, J. Phys. Chem. C 111 (2007) 6976–6982.
[23] A. Ghicov, J.M. Macak, H. Tsuchiya, J. Kunze, V. Haeublein, L. Frey, P. Schmuki, Nano Lett. 6 (2006) 1080–1082.
[24] T. Arai, M. Yanagida, Y. Konishi, Y. Iwasaki, H. Sugihara, K. Sayama, J. Phys. Chem. C 111 (2007) 7574–7577.
[25] R. Asahi, T. Morikawa, H. Irie, T. Ohwaki, Chem. Rev. 114 (2014) 9824–9852.
[26] S.K. Park, T.K. Yun, J.Y. Bae, J. Nanosci. Nanotech. 15 (2015) 5967–5970.
[27] D. Lozano, J.M. Hernández-López, P. Esbrit, M.A. Arenas, E. Gómez-Barrena, J. de Damborenea, J. Esteban, C. Pérez-Jorge, R. Pérez-Tanoira, A. Conde, J. Biomed. Mater. Res. Part A (2014).
[28] A. Giannakas, M. Antonopoulou, Y. Deligiannakis, I. Konstantinou, Appl. Catal. B: Environ. 140 (2013) 636–645.
[29] J.C. Yu, J. Yu, W. Ho, Z. Jiang, L. Zhang, Chem. Mater. 14 (2002) 3808–3816.
[30] J.C. Yu, W. Ho, J. Yu, H. Yip, P.K. Wong, J. Zhao, Environ. Sci. Tech. 39 (2005) 1175–1179.
[31] Y. Cong, J. Zhang, F. Chen, M. Anpo, D. He, J. Phys. Chem. C 111 (2007) 10618–10623.
[32] S.P. Tallósy, L. Janovák, J. Ménesi, E. Nagy, Á. Juhász, L. Balázs, I. Deme, N. Buzás, I. Dékány, Environ. Sci. Pollut. Res. (2014) 1–13.
[33] K. Lv, H. Zuo, J. Sun, K. Deng, S. Liu, X. Li, D. Wang, J. Hazard. Mater. 161 (2009) 396–401.
[34] S. In, A. Orlov, R. Berg, F. García, S. Pedrosa-Jimenez, M.S. Tikhov, D.S. Wright, R.M. Lambert, J. Am. Chem. Soc. 129 (2007) 13790–13791.
[35] H. Sun, S. Wang, H.M. Ang, M.O. Tadé, Q. Li, Chem. Eng. J. 162 (2010) 437–447.
[36] S. Song, J. Tu, Z. He, F. Hong, W. Liu, J. Chen, Appl. Catal. A: Gen. 378 (2010) 169–174.
[37] X. Hong, Z. Wang, W. Cai, F. Lu, J. Zhang, Y. Yang, N. Ma, Y. Liu, Chem. Mater. 17 (2005) 1548–1552.
[38] S. Usseglio, A. Damin, D. Scarano, S. Bordiga, A. Zecchina, C. Lamberti, J. Am. Chem. Soc. 129 (2007) 2822–2828.
[39] W. Su, Y. Zhang, Z. Li, L. Wu, X. Wang, J. Li, X. Fu, Langmuir 24 (2008) 3422–3428.
[40] S. Tojo, T. Tachikawa, M. Fujitsuka, T. Majima, J. Phys. Chem. C 112 (2008) 14948–14954.
[41] Y. Ma, J.-W. Fu, X. Tao, X. Li, J.-F. Chen, Appl. Surf. Sci. 257 (2011) 5046–5051.
[42] P. Xu, J. Lu, T. Xu, S. Gao, B. Huang, Y. Dai, J. Phys. Chem. C 114 (2010) 9510–9517.
[43] M. Long, W. Cai, Z. Wang, G. Liu, Chem. Phys. Lett. 420 (2006) 71–76.
[44] K. Yang, Y. Dai, B. Huang, M.-H. Whangbo, Chem. Mater. 20 (2008) 6528–6534.
[45] S. Ghosh, R. Kaushik, K. Nagalakshmi, S. Hoti, G. Menezes, B. Harish, H. Vasan, Carbohydr. Res. 345 (2010) 2220–2227.
[46] V. Štengl, T.M. Grygar, Int. J. Photoenergy 2011 (2011) 13, http://dx.doi.org/10.1155/2011/685935, Article ID 685935.
[47] V.V. Zhdankin, Hypervalent Iodine Chemistry, Wiley, West Sussex, 2014.
[48] L. Liu, W. Yang, Q. Li, S. Gao, J.K. Shang, ACS Appl. Mater. Interfaces 6 (2014) 5629–5639.
[49] Q. Li, Y.W. Li, Z. Liu, R. Xie, J.K. Shang, J. Mater. Chem. 20 (2010) 1068–1072.
[50] Q. Li, Y.W. Li, P. Wu, R. Xie, J.K. Shang, Adv. Mater. 20 (2008) 3717–3723.
[51] K.R. Kissell, K.B. Hartman, P.A. Van der Heide, L.J. Wilson, J. Phys. Chem. B 110 (2006) 17425–17429.
[52] Y. Ma, J.-W. Fu, X. Tao, X. Li, J.-F. Chen, Appl. Surf. Sci. 257 (2011) 5046–5051.
[53] X. Tan, Q. Fan, X. Wang, B. Grambow, Environ. Sci. Tech. 43 (2009) 3115–3121.
[54] B. Tian, R. Dong, J. Zhang, S. Bao, F. Yang, J. Zhang, Appl. Catal. B: Environ. 158–159 (2014) 76–84.
[55] H. Liu, W. Yang, Y. Ma, Y. Cao, J. Yao, J. Zhang, T. Hu, Langmuir 19 (2003) 3001–3005.
[56] E. McCafferty, J. Wightman, Surf. Interface Anal. 26 (1998) 549–564.
[57] S. Bagwasi, B. Tian, F. Chen, J. Zhang, Appl. Surf. Sci. 258 (2012) 3927–3935.
[58] G. Liu, Z. Chen, C. Dong, Y. Zhao, F. Li, G.Q. Lu, H.-M. Cheng, J. Phys. Chem. B 110 (2006) 20823–20828.
[59] Z. He, L. Xie, S. Song, C. Wang, J. Tu, F. Hong, Q. Liu, J. Chen, X. Xu, J. Mol. Catal. A: Chem. 319 (2010) 78–84.
[60] H. Fu, C. Pan, W. Yao, Y. Zhu, J. Phys. Chem. B 109 (2005) 22432–22439.
[61] T. Wu, G. Liu, J. Zhao, H. Hidaka, N. Serpone, J. Phys. Chem. B 102 (1998) 5845–5851.
[62] Q. Yang, L. Shuai, X. Pan, Biomacromolecules 9 (2008) 3422–3426.
[63] W. Wang, Y. Yu, T. An, G. Li, H.Y. Yip, J.C. Yu, P.K. Wong, Environ. Sci. Tech. 46 (2012) 4599–4606.
[64] A. Ye, W. Fan, Q. Zhang, W. Deng, Y. Wang, Catal. Sci. Tech. 2 (2012) 969–978.
[65] J. Yu, J. Jin, B. Cheng, M. Jaroniec, J. Mater. Chem. A 2 (2014) 3407–3416.
[66] P.K. Stoimenov, V. Zaikovski, K.J. Klabunde, J. Am. Chem. Soc. 125 (2003) 12907–12913.
[67] W. Wang, J. Yu, Q. Xiang, B. Cheng, Appl. Catal. B: Environ 119–120 (2012) 109–116.